International Journal of Automotive Technology, Vol. 18, No. 5, pp. 911–922 (2017)
DOI 10.1007/s12239–017–0089–2

pISSN 1229–9138/ eISSN 1976–3832

MODELING AND CONTROL OF ENGINE STARTING FOR A FULL HYBRID ELECTRIC VEHICLE BASED ON SYSTEM DYNAMIC CHARACTERISTICS

Yonggang Liu[1, 2)*], Daqi Chen[1)], Zhenzhen Lei[1)], Datong Qin[1)], Yi Zhang[3)], Rui Wu[1)] and Yong Luo[2)]

[1)]State Key Laboratory of Mechanical Transmissions & School of Automotive Engineering, Chongqing University, Chongqing 400044, China
[2)]Key Laboratory of Advanced Manufacture Technology for Automobile Parts, Ministry of Education, Chongqing University of Technology, Chongqing 400054, China
[3)]Department of Mechanical Engineering, University of Michigan-Dearborn, MI 48128, USA

(Received 28 October 2016; Revised 6 February 2017; Accepted 17 February 2017)

ABSTRACT–This paper focuses on the dynamic modeling and control of engine starting for a Full Hybrid Electric Vehicle (FHEV) consisting of an Integrated Starter Generator (ISG) and Dual Clutch Transmissions (DCTs). The dynamic characteristics of the engine, the ISG motor and the main clutch are analyzed respectively. The dynamic models of the main components of the powertrain system are also established taking the system dynamic characteristics into consideration. The FHEV dynamic model of engine starting during electric driving mode has been investigated in detail. The coordinated control strategy of engine starting has been proposed based on the powertrain system dynamic characteristics. The simulation for the engine starting control during electric driving mode has been performed based on the Matlab/Simulink platform. The simulation results show that the proposed control strategy satisfies the requirements of response and smoothness during engine starting process. Furthermore, a bench test has been carried out to analyze the system characteristics during engine starting process. The test data is highly agreeable to the simulation data and the effectiveness of engine starting control strategy is validated by the comparison between simulation results and the test data.

KEY WORDS : Hybrid electric vehicle, Dual clutch transmissions, Modeling, Simulation, Experiment

NOMENCLATURE

$\dot{m}_a$: rate of air mass flow in manifold and port passage
$\dot{m}_{at}$: air mass flow rate past throttle plate
$\dot{m}_{ap}$: air mass flow rate into cylinder
$\dot{m}_{fi}$: injected fuel mass flow
$\dot{m}_f$: cylinder port fuel mass flow
$\dot{m}_{ff}$: fuel film mass flow
$\dot{m}_{fv}$: fuel vapor mass flow
c_t : flow coefficient of throttle body throat
α : is the throttle plate angle
V_m : volume of manifold and port passage
T_i : engine indicated torque
T_{load} : engine loading torque
θ : spark advance angle
η_i : engine indicated efficiency
λ : air/fuel ratio
H_u : low BTU of fuel
V_d : d-axis voltage
V_q : q-axis voltage
i_d : d-axis current
i_q : q-axis current
L_d : d-axis inductance
L_q : q-axis inductance
p : pole pairs of permanent magnet synchronous motor
ψ_m : magnet flux of permanent magnet synchronous motor
Φ_m : magnet flux
H_m : magnet field intensity
L_m : of magnetic circuit
x_s : armature displacement
x_{s0} : initial compression displacement of the HSV return spring
Q_{in} : average flow of supplying port
Q_{out} : average flow of recycle port
Q_{net} : net flow from the HSV to hydraulic cylinder
τ : duty ratio
x_p : hydraulic cylinder piston displacement

SUBSCRIPTS

driven : main clutch driven plate
driving : main clutch driving plate
w : wheel

**Corresponding author.* e-mail: andylyg@umich.edu

L : loading
C0 : main clutch
e : engine

1. INTRODUCTION

Along with the oil resource being used up and the environment pollution problem becoming more serious, Hybrid Electric Vehicles (HEVs) have become the most effective solution to energy saving and environment protection. Hybrid Electric Vehicles have much more flexible driving patterns since it has two power sources, engine as well as motor. With the combination of different operating states of engine and motor, HEVs have different driving modes and can transfer the driving modes according to the vehicle driving condition (Somayajula *et al*., 2009; Ahn and Cha, 2008). Recently, the researches on HEVs mode transition process are mainly based on the traditional modeling without considering the influence of dynamic characteristics of powertrain system. Actually, the dynamic characteristics of driving components have obvious influence on the mode transition process. Therefore, the driving mode transition control considering system dynamic characteristics is the key factor of improvement of mode transition performance.

In terms of dynamic modeling of powertrain system, 1) a Mean Value Engine Model (MVEM) based on mathematical and parametric equations has been developed and the simulation results of mass flow rate and manifold pressure are validated with experimental data (Asl *et al*., 2013). A systematic model reduction approaches for mean value model of a diesel engine is developed and the accuracy of the reduced models is validated through extensive simulation and engine test data (Broomhead *et al*., 2015). A mean value model for a turbocharged diesel engine based on the Design of Experiments (DOE) and hybrid Radial Basis Functions (RBF) has been developed, which realizes a good trade-off of model accuracy and run speed (He and Lin, 2007). The air path MVEM modeling method based on the 1D detail model is discussed for a turbocharged diesel engine (Wu *et al*., 2011). The mass flow rate and temperature of the air system in the diesel engines are modeled with consideration of physical phenomena and the thermodynamic law to estimate the exhaust pressure accurately (Lee *et al*., 2014). The mean value of central fuel injection (CFI) engine model is researched and the engine variables are identified (Hendricks and Sorenson, 1990; Hendricks and Vesterholm, 1992; Hendricks *et al*., 1992, 1996), which provide theoretical foundation for the dynamic modeling of engine. 2) Direct torque control of interior permanent magnet synchronous motors is carried out and the simulation results show that the control system have good dynamic and static characteristics, which provides a reference for dynamic modeling of motor (Meng *et al*., 2013). The dynamic characteristics of the torque and speed of the Permanent Magnet Brushless DC Motor is discussed in start-go mode of operation with abrupt change of required load torque (Ke *et al*., 2008). The dynamic torque response of motor is measured through the simulation and HIL implementation with vehicle driving cycles (Oh, 2005). A space vector current controller for a brushless permanent magnet motor in hybrid electric vehicles is proposed to decrease the current ripple, which improves the performance of the brushless PM machine drive (Kim and Vodyakho, 2009). 3) The dynamic models and transfer function of hydraulic actuator system of clutch used for heavy-duty automatic transmission are established and the clutch actuator model is validated to predict the dynamic behavior of the shift hydraulic system with high accuracy by comparing the experimental and simulation results (Meng *et al*., 2015). A dynamic modeling method for a solenoid actuator system is proposed, which realizes the precise predictions of a hydraulic valve pressure and is validated through a test (Manyala and Atashbar, 2013). The dynamic mathematical model and the dynamic characteristic of the electro-hydraulic variable valve system are derived, which lays theoretical foundation for the dynamic modeling of hydraulic actuator system of main clutch (Liu *et al*., 2009). The models of the hydraulic system using pulse width modulation (PWM) method in automatic transmissions are established and the characteristics of solenoid valve are tested using different duty ratio (Cho *et al*., 2002).

There are many researches on the HEVs driving mode transition. The engine starting control for HEVs is researched and the coordinated torque control of motor and clutch with the closed loop strategy is proposed, which are validated through a bench test (Smith *et al*., 2011). In order to reduce the torque fluctuation during the mode transition, a torque disturbance observer is designed to improve the accuracy and performance of control system (Kim *et al*., 2011). A coordinated control strategy of motor torque for mode transition for dual-mode power split HEVs is simulated, which is effective to reduce the torque fluctuation (Ma *et al*., 2015). A four-phase control strategy for parallel HEVs during mode transition from the electric vehicle mode to the hybrid mode is analyzed and the mode transition performance has been improved effectively (Song *et al*., 2012).

These researches on HEV mode transition process are mostly based on the static modeling of powertrain system without considering the dynamic characteristics. However, the dynamic characteristics of powertrain system have great influence on the response and torque fluctuation during mode transition process. Therefore, the systematic analysis of dynamic characteristics of powertrain system, including the engine, the motor and the clutch actuator, is essential to improve mode transition performance, which hasn't been seen in the present literatures.

The configuration of FHEV is shown in Figure 1. The main components of the hybrid powertrain system include an engine, a main clutch, an ISG motor, batteries and DCT.

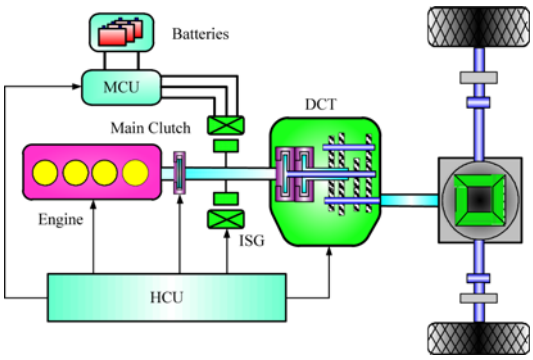

Figure 1. Configuration of a FHEV with an ISG.

There are two power sources which are the engine and the motor. The function of the main clutch is to engage or disengage the engine from the powertrain of the FHEV. Therefore, this FHEV system can realize all the working modes by controlling the engine, the motor and the main clutch. This type of HEV powertrain system features a simple structure, a low cost and a high efficiency.

In this paper, engine starting control of the FHEV during electric driving mode is discussed considering system dynamic characteristics. Firstly, the dynamic characteristics of engine, ISG motor and wet multi-plate clutch have been analyzed and the dynamic models of those components of powertrain system have been established respectively. Secondly, the systematic analysis of dynamic characteristics during engine starting process has been presented and the coordinated control strategy for engine starting has been proposed. At last, the simulation and bench test of the engine starting control have been carried out. The simulation and experimental results show that the dynamic model can better reflect the dynamic characteristics of the powertrain system and have better consistency to the test results, which provides a theoretical basis for the mode transition strategy and improving the mode transition performance.

2. ENGINE DYNAMIC CHARACTERISITCS

2.1. Dynamic Modeling of Engine

The dynamic characteristics of engine have been researched based on the mean value engine model. The mean value engine model describes the air mass flow in intake manifold and exhaust manifold as well as the dynamic changes of temperature of air/fuel mixture using an ordinary differential equation (ODE) based on the mass and energy conservation. The model also describes the air pressure changes by ideal gas state equation. The described parameters of engine above are all a mean value in a period of time. A mean value engine model consists of three dynamic subsystems, intake manifold air mass flow subsystem, fuel vapor and fuel film subsystem, and crank shaft and loading subsystem.

2.1.1. Intake manifold air mass flow subsystem

The intake manifold air mass flow model is established to calculate the engine input air by engine state variables (such as engine speed, throttle opening, etc.). The intake manifold air mass flow model consists of throttle model, intake valve model and intake manifold internal pressure model.

The throttle model is described as follows.

$$\begin{cases} \dot{m}_{at}(\alpha, P_m) = \dfrac{\pi}{4} c_t D^2 \dfrac{P_{am}\sqrt{k'}}{\sqrt{Rt_{am}}} \beta_1(\alpha)\beta_2(P_m) + \dot{m}_{at0} \\ k' = \dfrac{2k}{k-1} \\ \beta_1(\alpha) = 1-\cos(\alpha-\alpha_0) \\ \beta_2(P_m) = \sqrt{P_r^{\frac{2}{k}} - P_r^{\frac{k+1}{k}}} \\ P_r = \max\left(\dfrac{P_m}{P_{am}}, \left(\dfrac{2}{k+1}\right)^{\frac{k}{k-1}}\right) \end{cases} \tag{1}$$

Where, D is the diameter of throttle body throat, $\dot{m}_{at}$ is the air mass flow rate past throttle plate, α is the throttle plate angle, P_m is the manifold air pressure, c_t is the flow coefficient of throttle body throat, P_{am} is the ambient pressure, t_{am} is the ambient temperature, R is the gas constant, and k is the ratio of the specific heats.

The intake valve model is described as follows.

$$\dot{m}_{ap} = \frac{n_e V_e P_m \eta_c}{120 R t_m} = \frac{n_e V_e}{120 R t_m}(S_i P_m - y_i) \tag{2}$$

Where, $\dot{m}_{ap}$ is the air mass flow rate into cylinder, n_e is the engine speed, V_e is the engine displacement, t_m is the intake manifold temperature and η_c is the volumetric efficiency.

The Equation (2) is improved by Hendricks in terms of $P_m\eta_c = (S_iP_m - y_i)$. For the single valve gasoline engine, S_i and y_i are approximately both constants. Hence, the S_i and y_i are 0.952 and 0.097 respectively.

The intake manifold internal pressure model is described as follows.

$$\begin{cases} \dot{m}_a = \dot{m}_{at} - \dot{m}_{ap} \\ \dot{P}_m = \dfrac{Rt_m}{V_m}\dot{m}_a \end{cases} \tag{3}$$

Where, $\dot{m}_a$ is the change rate of air mass flow in manifold and port passage and V_m is the volume of manifold and port passage.

2.1.2. Fuel vapor and fuel film model

Fuel vapor and fuel film model is presented to calculate the actual injection quantity in cylinder. The fuel mass flow has two ways to be sprayed into the cylinder to burn after injection from the injector. One way is that the injected fuel in the form of vapor combines with the air and then the fuel

mixture burns in the cylinder. The other way is that the fuel film which is attached to manifold evaporates again and then the evaporated fuel vapor burns in the cylinder. The fuel vapor and fuel film model is described as follows.

$$\begin{cases} \dot{m}_{fv} = (1-x)\dot{m}_{fi} \\ \dot{m}_{ff} = \dfrac{1}{\tau_u}(x\dot{m}_{fi} - \dot{m}_{ff}) \\ \dot{m}_f = \dot{m}_{fv} + \dot{m}_{ff} \end{cases} \tag{4}$$

Where, x is the fraction of the injected fuel which is attached to manifold as fuel film, $(1 - x)$ is the fraction of the injected fuel which is attached to manifold as fuel vapor, τ_u is the time constant of fuel evaporation, $\dot{m}_{fv}$ is the fuel vapor mass flow, $\dot{m}_{fi}$ is the injected fuel mass flow, $\dot{m}_{ff}$ is the fuel film mass flow and $\dot{m}_f$ is the cylinder port fuel mass flow.

The x and τ_u can be obtained from the nonlinear fuel film dynamic compensator calibration experiment. For simultaneous multipoint injection (MFI) engine, x and τ_u are approximately constants at normal temperature, x is 0.22 and τ_u is 0.25 s.

2.1.3. Crank shaft and loading model

The crank shaft and loading model is presented to calculate the engine output torque according to the cylinder port fuel mass flow and other variables (such as excessive air coefficient, intake manifold air pressure, spark advance angle, etc.) calculated by the two models above. The crank shaft and loading model is described as follows.

$$\begin{cases} T_i = \dfrac{H_u \eta_i \dot{m}_f(t-\tau_d)}{n_e} \\ \dot{n}_e = \dfrac{T_e - T_{load}}{I_e} \\ T_e = T_i - \dfrac{\Sigma P_{loss}}{n_e} \\ \eta_i(n_e, P_m, \lambda, \theta) = \eta_i(n_e)\cdot\eta_i(P_m)\cdot\eta_i(\lambda)\cdot\eta_i(\theta) \\ \eta_i(n_e) = \eta_{i0} - \eta_{in} e^{\frac{-n_e}{n_0}} \\ \eta_i(P_m) = P_{m0} + P_{m1}P_m + P_{m2}P_m^2 \\ \eta_i(\lambda, n_e) = a_0 + a_1\lambda + a_2\lambda^2 + a_3 n_e \\ \eta_i(\theta, n_e) = k_0 + k_1(\theta - (k_2 n_e + k_3))^2 \end{cases} \tag{5}$$

Where, T_i is the engine indicated torque, H_u is the low BTU of fuel, τ_d is the time delay of fuel burning, T_e is the engine effective torque, T_{load} is the loading torque, I_e is the moment of inertia of crank shaft, $\sum P_{loss}$ is the pumping and frictional loss, λ is the air/fuel ratio, θ is the spark advance angle, and η_i is the engine indicated efficiency, which is ratio of actual cycle indicated power to the thermal efficiency. The engine indicated efficiency is influenced by engine speed, intake manifold air pressure and spark advance angle and it is the function of the four variables above.

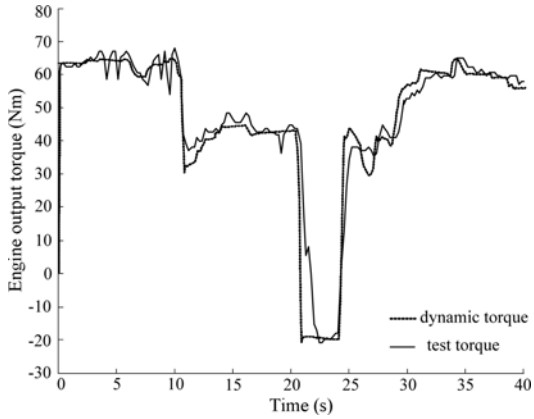

Figure 2. Comparison results of the engine characteristic.

2.2. Engine Torque Response Simulation and Test

In order to verify the proposed engine model, the mean value engine model has been established based on Matlab/Simulink platform. Furthermore, a prototype vehicle test has been performed. The throttle opening signal is obtained during the real test to verify the proposed MVEM as an input signal. The simulation results are compared with the real vehicle test data and the comparison results of engine output torque are shown in Figure 2.

Figure 2 illustrates that the dynamic characteristic of engine output torque between simulation and test data. The response time of engine output torque from 0 to 64 Nm is approximately 0.28 s. The abrupt changes of throttle opening (such as about 10 s, 20 s and 25 s) result in a fast change of air mass flow rate through throttle plate. However, the change of air mass flow rate of cylinder doesn't take place immediately due to the characteristics of intake manifold. As a result, there will be a slight overshoot of engine torque as shown in Figure 2. In general, the engine output torque from simulation is agreeable with the real vehicle test data. Therefore, the effectiveness of the proposed dynamic engine model is validated by the comparison between simulation results and the test data.

3. ISG DYNAMIC CHARACTERISITCS

3.1. Dynamic Modeling of ISG Motor

The permanent magnet synchronous motor (PMSM) is used in this study. Compared with vector control, direct torque control (DTC) of motor is simple in structure and features the excellent performance of both static and dynamic control. The dynamic mathematical model of ISG motor is established as follows according to the ISG motor structure and DTC of ISG motor.

$$\begin{cases} V_{\mathrm{d}} = R_0 i_{\mathrm{d}} + L_{\mathrm{d}} \dfrac{di_{\mathrm{d}}}{dt} - p\omega_m L_{\mathrm{q}} i_{\mathrm{q}} \\ V_{\mathrm{q}} = R_0 i_{\mathrm{q}} + L_{\mathrm{q}} \dfrac{di_{\mathrm{q}}}{dt} + p\omega_m L_{\mathrm{d}} i_{\mathrm{d}} + p\omega_m \Psi_{\mathrm{m}} \\ M_{\mathrm{m}} = \dfrac{3p}{2}(\Psi_{\mathrm{m}} i_{\mathrm{q}} + (L_{\mathrm{d}} - L_{\mathrm{q}}) i_{\mathrm{d}} i_{\mathrm{q}}) \\ M_{\mathrm{m}} - M_{\mathrm{load}} - M_{\mathrm{f}} = J_{\mathrm{m}} \dfrac{d\omega_{\mathrm{m}}}{dt} \\ \omega_{\mathrm{ele}} = \dfrac{d\theta_{\mathrm{e}}}{dt} = p\omega_{\mathrm{m}} \end{cases} \tag{6}$$

Where, V_{d} is the d-axis voltage, V_{q} is the q-axis voltage, i_{d} is the d-axis current, i_{q} is the q-axis current, L_{d} is the d-axis inductance, L_{q} is the q-axis inductance, p is the pole pairs of permanent magnet synchronous motor, ψ_{m} is the magnet flux of permanent magnet synchronous motor, M_{m} is the output torque of permanent magnet synchronous motor, M_{load} is the loading torque, M_{f} is the friction torque of permanent magnet synchronous motor, J_{m} is equivalent moment of inertia of the powertrain components converted to the output shaft of permanent magnet synchronous motor, ω_{m} is the rotate speed of rotor and ω_{ele} is the electromagnetic angle velocity.

3.2. ISG Motor Torque Response Simulation and Test

The ISG motor has two working modes including speed control mode and torque control mode. The control of engine starting during electric driving process is mainly based on the coordinated torque control between engine and motor. Therefore, this paper only focuses on the output torque response characteristics of ISG motor.

3.2.1. ISG motor torque response simulation

The response performance of ISG motor is evaluated by the response time and accuracy of output torque. The ISG motor simulation model is established based on Matlab/ Simulink platform and the simulation results of ISG torque response are shown in Figure 3.

As shown in Figure 3, the output torque of ISG motor can follow the target torque quickly with up or down step excitation signal. The response time is approximately 25 ms. The simulation results represent the dynamic characteristic of ISG motor torque in terms of response and overshoot. Therefore, the proposed model of PMSM is suitable for the research on the control of engine starting process.

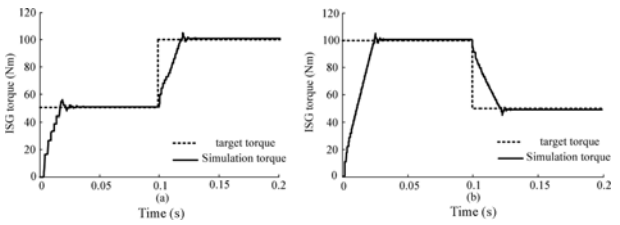

Figure 3. Simulation of ISG motor torque response.

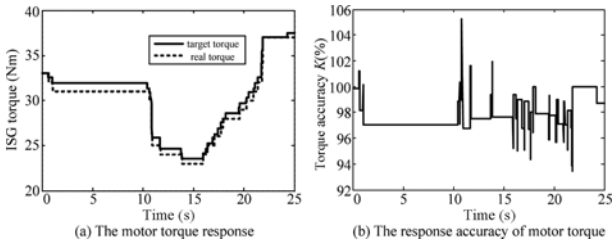

Figure 4. Test results of ISG motor torque.

3.2.2. ISG motor torque response test

In order to verify the torque response of ISG motor, an ISG motor torque bench test has been implemented and the test results are shown in Figure 4.

The Figure 4 (a) illustrates that the ISG motor torque can follow the target torque quickly in the direct torque control mode. K in Figure 4 (b) is the ratio of real torque and target torque. The response time is within 30 ms and the torque accuracy K is above 96 percent in most test period. As shown in Figure 4, the proposed ISG motor model can meet the requirement of torque response. The accuracy of dynamic model of ISG motor is validated through the results of torque response test.

4. MAIN CLUTCH DYNAMIC CHARACTERISITCS

The main clutch is a key component of powertrain system, which directly decides the operation mode of vehicles through its engagement and disengagement. The function of the main clutch is to apply or release the engine from the powertrain of the FHEV. The dynamic characteristics of main clutch directly influence mode transition performance. The wet multi-plate clutch is chosen as the main clutch and the main clutch characteristics are mainly decided by the with hydraulic actuator system.

The layout of the hydraulic system of the main clutch is shown in the Figure 5. A high-speed solenoid valve (HSV)

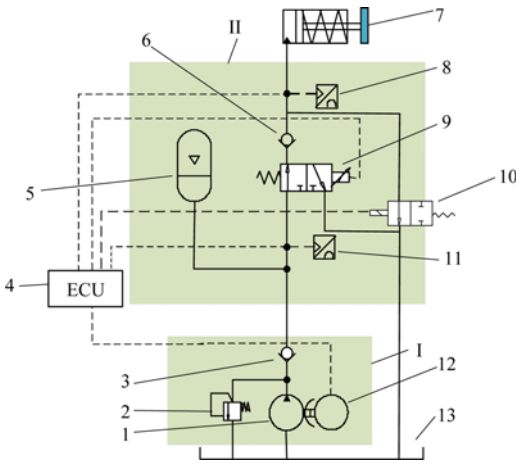

Figure 5. Layout of hydraulic system of main clutch.

has been used for the hydraulic cylinder pressure control. The actuator system consists of hydraulic power source I, pressure control system II, main clutch hydraulic cylinder 7 and Electronic Control Unit (ECU) 4. The hydraulic power source I consists of hydraulic pump 1, relief valve 2, one-way valve 3, motor 12 and hydraulic fuel tank 13. The pressure control system II consists of accumulator 5, one-way valve 6, pressure sensor 8, 11, HSV 9 and reversing valve 10.

During the engagement of the main clutch, the HSV 9 controlled by ECU will be powered on and reversing valve 10 will be powered off. The hydraulic fuel is pumped out from hydraulic fuel tank 13 and the hydraulic fuel flows into the hydraulic cylinder 7 through hydraulic pump 1, one-way valve 3 and HSV 9 sequentially. The pressure of hydraulic cylinder 7 is controlled by the HSV 9 through the duty ratio of Pulse-width Modulating (PWM) of HSV. As a result, the main clutch torque will be changed with the variation of hydraulic cylinder pressure. Vice versa, the pressure of the hydraulic cylinder is also decided by the HSV 9. Therefore, the main clutch dynamic characteristics are mainly influenced by the HSV and hydraulic cylinder.

4.1. High-speed Solenoid Valve Modeling

In order to accurately control the hydraulic cylinder pressure, the duty ratio of PWM for HSV is needed to be controlled precisely. As well known, the duty ratio is achieved by the switching state of valve port of HSV to change the rate of flow of hydraulic fuel. The two-position and three-port solenoid valve controlled by PWM is used, which is a normal closed type with fast response switching digital valve. The valve directly receives the digital signal to control the pressure and flow of hydraulic system with PWM control. The PWM high-speed solenoid valve model mainly consists of magnetic circuit model, ball valve model and fluid model.

The function of magnetic circuit model is to calculate the magnetic force acted on the armature of HSV based on the Kirchhoff laws and Maxwell equation. The magnetic circuit model is described as follows.

$$\begin{cases} iN = \Phi_m R_\delta + H_m L_m \\ R_\delta = (g_{max} - x_s + g_{ser})/u_0 A \\ \Phi_m = \int \dfrac{(U - iR_{cir})}{N} \\ B_m = \Phi_m / A \\ i = (\Phi_m R_\delta + H_m L_m)/N \\ F_{mag} = \Phi_m^2/(2u_0 A) \end{cases} \tag{7}$$

Where, i is the current, N is the inductor coil turns, Φ_m is the magnet flux, R_δ is the resistance of work air gap, H_m is the magnet field intensity, L_m is the length of magnetic circuit, g_{max} is the max air gap length, g_{ser} is the series equivalent air gap, x_s is the armature displacement, u_0 is the permeability of vacuum, A is the magnet pole area, U is the input voltage, R_{cir} is the resistance of magnet circuit, F_{mag} is the magnet force acted on the armature and B_m is the magnetic induction strength of the circuit.

The magnetic force acted on the armature of HSV increases as the increase of current during engagement. After the armature begins to move, the ball valve moves due to the link between ball valve and armature. Therefore, the movement of ball valve realizes the switching of valve port. When the duty ratio signal is received, the duty ratio is realized through the switching frequency of valve port. The ball valve model is descried as follows.

$$\begin{cases} \ddot{x}_s = (F_{mag} + F_s - F_{sp} - F_h)/m_s \\ F_s = A_0 p_s \\ F_{sp} = K_s(x_s + x_{s0}) \\ F_h = C_v \dot{x}_s \\ x_s = \iint (F_{mag} + F_s - F_{sp} - F_h)/m_s \end{cases} \tag{8}$$

Where, x_s is the ball valve displacement, m_s is the mass of ball valve, F_s is the front pressure that is acted on the ball valve by the entry port hydraulic oil, F_{sp} is the force of return spring that is acted on the ball valve, F_h is the viscous damping force of hydraulic oil, A_0 is the cross-sectional area of ball valve, p_s is the pressure of supplying port, C_v is the viscous damping coefficient of hydraulic oil in the HSV, K_s is the is the stiffness of return spring of HSV and x_{s0} is the initial compression displacement of the return spring.

The supplying port and working port open due to the movement of ball valve. A part of hydraulic oil flows into the working port and the remaining oil flows into recycle port. Since the working port is connected to hydraulic cylinder, the piston of hydraulic cylinder is moved by the hydraulic pressure from working port. The fluid model is descried as follows.

$$\begin{cases} Q_{in} = \tau sign(p_s - p_c) C_d A_d \sqrt{2(p_s - p_c)/\rho} \\ Q_{out} = (1 - \tau)\text{sign}(p_c) C_d A_d \sqrt{2p_c/\rho} \\ Q_{net} = Q_{in} - Q_{out} \end{cases} \tag{9}$$

where, Q_{in} is the average flow of supplying port, Q_{out} is the average flow of recycle port, Q_{net} is the net flow that is from the high speed solenoid valve to hydraulic cylinder, C_d is the solenoid valve flow coefficient, A_d is the solenoid valve throttling area, ρ is the density of hydraulic oil, p_c is the control pressure of hydraulic cylinder and τ is the duty ratio.

4.2. Modeling of Hydraulic Actuator of Main Clutch

The engagement of main clutch contains three phases. 1) When the hydraulic cylinder piston displacement x_p is less than clearance of friction plates δ, the free travel of main clutch is eliminated gradually with the increase of movement of piston. The piston pushes the friction compression plates with hydraulic pressure. 2) When the x_p exceeds the

clearance of friction plates δ, the clearance of friction plates is eliminated completely. The main clutch is in slipping state with increases of piston displacement. The clutch is transmitting torque during the slipping state. 3) The engagement is implemented and the hydraulic cylinder piston displacement is maintained when the speed of driven plates approaches the speed of driving plates. The hydraulic cylinder piston displacement model is described as follows during the engagement of main clutch.

$$\begin{cases} m_{\mathrm{p}}\ddot{x}_{\mathrm{p}} = p_{\mathrm{c}}A_{\mathrm{p}} - K_{\mathrm{p}}(x_{\mathrm{p}} + x_{\mathrm{p0}}) - B_0\dot{x}_{\mathrm{p}} \\ \dfrac{dp_{\mathrm{c}}}{dt} = \dfrac{\beta}{V_0}(Q_{\mathrm{net}} - \dot{x}_{\mathrm{p}}A_{\mathrm{p}}) \end{cases} \tag{10}$$

Where, β is the hydraulic oil bulk modulus, x_{p} is the hydraulic cylinder piston displacement, A_{p} is the cross-sectional area of the piston, m_{p} is the mass of piston, K_{p} is the return spring stiffness, x_{p0} is the initial compression displacement of the return spring, B_0 is the viscous damping coefficient of hydraulic oil in the cylinder, V_0 is the sum of hydraulic cylinder initial volume and the volume from the high speed solenoid valve work outlet to hydraulic cylinder supplying oil pipe.

The transfer function of hydraulic actuator of main clutch can be derived from the fluid model and piston displacement model, which can represent the dynamic characteristics of main clutch. The clutch transmitted torque can follow the target torque through the precise hydraulic pressure control. The hydraulic pressure control can be realized through the piston displacement control based on the piston displacement model. As a results, the clutch transmitted torque can be controlled through the piston displacement control. In order to obtain the transfer function that the input is duty ratio τ and the output is piston displacement x_{p}, the fluid model Equation (9) is needed to be linearized at first based on the Taylor expansion at the operating point (τ_0, P_{c0}, Q_{net0}) with ignoring the higher order infinitesimal. The Taylor expansion equations are described as follows.

$$\begin{aligned} \Delta Q_{\mathrm{net}} &= \left(\frac{\partial f}{\partial \tau}\right)_{\tau_0,\mathrm{Pc0}} \Delta\tau + \left(\frac{\partial f}{\partial p_c}\right)_{\tau_0,\mathrm{Pc0}} \Delta p_{\mathrm{c}} \\ k_1 = \left(\frac{\partial f}{\partial \tau}\right)_{\tau_0,\mathrm{Pc0}} &= sign(p_{\mathrm{s}} - p_{\mathrm{c0}})C_{\mathrm{d}}A_{\mathrm{d}}\sqrt{2(p_{\mathrm{s}} - p_{\mathrm{c0}})/\rho} + \\ & C_{\mathrm{d}}A_{\mathrm{d}}\sqrt{2p_{\mathrm{c0}}/\rho} \\ k_2 = \left(\frac{\partial f}{\partial p_{\mathrm{c}}}\right)_{\tau_0,\mathrm{Pc0}} &= -\tau_0 sign(p_{\mathrm{s}} - p_{\mathrm{c0}})C_{\mathrm{d}}A_{\mathrm{d}}/\sqrt{2\rho(p_{\mathrm{s}} - p_{\mathrm{c0}})} \\ & -(1-\tau_0)C_dA_d/\sqrt{2p_{\mathrm{c0}}\rho} \end{aligned} \tag{11}$$

Supposing $\Delta Q_{\mathrm{net}} = Q_{\mathrm{net}}$, $\Delta\tau = \tau$, and $\Delta p = p$, the fluid model equation of HSV at the steady operating point is linear, which can be described as follows.

$$Q_{\mathrm{net}} = k_1\tau - k_2 p_{\mathrm{c}} \tag{12}$$

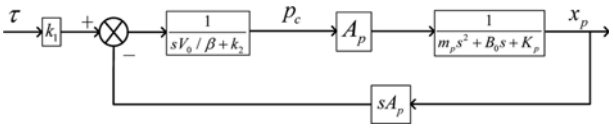

Figure 6. Block diagram of transfer function.

Through the Laplace transformation of fluid Equation (10), the hydraulic actuator transfer function block diagram has been obtained as shown in Figure 6.

In the Figure 6, the input is duty ratio τ and output is piston displacement x_p. The transfer function can be obtained as follows.

$$\frac{x_{\mathrm{p}}}{\tau} = \frac{A_{\mathrm{p}}\beta k_1}{(sV_0 + k_2\beta)\left(m_{\mathrm{p}}s^2 + B_0 s + K_{\mathrm{p}} + \dfrac{sA_p^2\beta}{sV_0 + k_2\beta}\right)} \tag{13}$$

As illustrated in the Equation (13), the transfer function of the clutch hydraulic actuator is a three-order system considering the hydraulic oil damping, return spring stiffness and hydraulic oil bulk modulus, etc.

4.3. Simulation of Hydraulic Actuator Dynamic Response

4.3.1. PWM high speed solenoid valve characteristics simulation

The dynamic response performance of high speed solenoid valve can be reflected by the dynamic response of magnet circuit current and ball valve displacement on the condition of different duty ratio of PWM signal. The dynamic response simulation of HSV has been implemented with 60 % duty ratio and 14V input pulsed voltage. The simulation results are illustrated in Figure 7.

As shown in Figure 7, the response of ball valve displacement is synchronized with the response of circuit current, which indicates the dynamic response of high speed solenoid valve can track the pulsed signal well. The

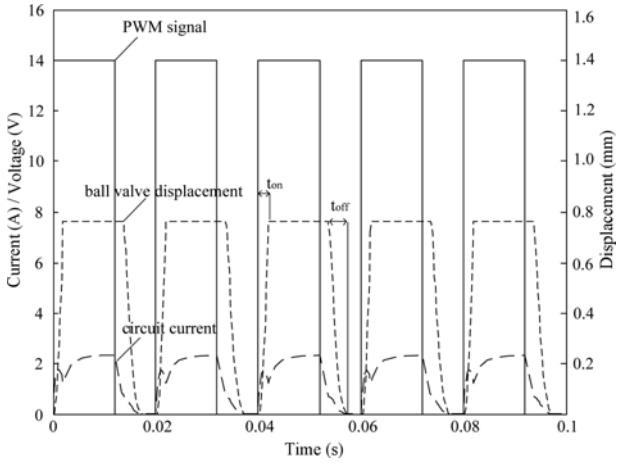

Figure 7. Dynamic response curse of high speed solenoid valve.

dynamic response of ball valve displacement always lags behind the PWM signal inevitably. The simulation results shows the high speed solenoid valve's opening time ton approximately equals to the closing time toff (4 ms), which proves the proposed high speed solenoid valve model has a great dynamic response performance of tracking the duty ratio signal. Therefore, the model of HSV proposed is validated to reflect dynamic characteristics of main clutch.

4.3.2. Hydraulic cylinder piston displacement characteristics simulation

The simulation of clutch hydraulic cylinder piston has been established using the Matlab/Simulink as a platform. The piston displacement curve is described in the Figure 8.

The Figure 8 shows the response time of piston displacement is about 0.11 s and the piston displacement curve meet the required value well after 0.11 s. The maximum overshoot of piston displacement is within 0.05 mm. The piston has a great performance of tracking the target displacement, which validated the hydraulic oil pressure of hydraulic cylinder can track the target pressure. As well known, the clutch transmitted torque is mainly decided by the clutch hydraulic oil pressure at given clutch structure. As a result, the clutch transmitted torque can follow the target torque through the precise piston displacement control. Moreover, the results show that output hydraulic oil pressure of the solenoid valve acts on the piston timely and the free travel of hydraulic cylinder piston can be eliminated quickly due to the fast response characteristics of actuator system. As a result, the main clutch dynamic characteristics mainly influenced by hydraulic actuator are validated through the HSV and piston displacement response simulation.

5. MODELING AND COORDINATED CONTROL FOR ENGINE STARTING

The researches on the control of mode transition are mainly based on traditional modeling of powertrain system in existing literatures, without taking the system dynamic characteristics into consideration. An effective coordinated control strategy has been proposed for engine starting process taking dynamic characteristics of powertrain system into consideration based on the validated models in Sections 2 ~ 4.

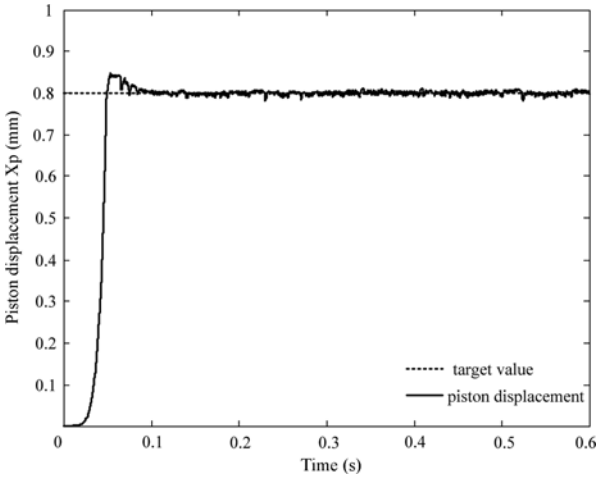

Figure 8. Dynamic response of piston displacement.

5.1. Dynamic Model of Engine Starting during Electric Driving Mode

The dynamic models of key components of powertrain system have been established before, which provides the foundation for dynamic analysis of mode transition of FHEV. The engine starting during electric driving mode has been chosen as an example to analyze the system dynamic characteristics. The dynamic model of engine starting of the FHEV is illuminated in Figure 9.

The system equations of motion for engine starting during electric driving mode can be described as follows.

$$\begin{cases} T_{\mathrm{e}} - T_{\mathrm{c0}} = I_{\mathrm{e}} \cdot \dot{\omega}_{\mathrm{e}} \\ T_{\mathrm{w}} = (T_{\mathrm{m}} - T_{\mathrm{c0}} - I_{\mathrm{m}} \cdot \dot{\omega}_{\mathrm{m}}) \cdot i_{\mathrm{DCT}} \cdot i_{\mathrm{a}} \cdot \eta_{\mathrm{t}} \\ T_{\mathrm{w}} - T_{\mathrm{L}} = I_{\mathrm{w}} \cdot \dot{\omega}_{\mathrm{w}} \end{cases} \tag{14}$$

Where, T_{c0} is the main clutch transmitted torque, T_{e} is the engine drag torque before engine ignition or engine output torque after engine ignition, I_{e} is the engine equivalent moment of inertia, ω_{e} is the engine speed, T_{m} is the ISG torque, I_{m} is the ISG equivalent moment of inertia, ω_{m} is the ISG speed, i_{a} is the main gear ratio, i_{DCT} is the gear ratio of DCT, η_{t} is the transmission efficiency of DCT, T_{w} is the wheel torque, T_{L} is the loading torque, I_{w} is equivalent moment of inertia of the powertrain components converted to the wheel and ω_{w} is the wheel speed.

After the full engagement of the main clutch, the engine speed is the same as ISG motor speed and the system equations of motion can be described as follows.

$$\begin{cases} T_{\mathrm{w}} = (T_{\mathrm{m}} + T_{\mathrm{e}} - I_{\mathrm{m}} \cdot \dot{\omega}_{\mathrm{m}} - I_{\mathrm{e}} \cdot \dot{\omega}_{\mathrm{e}}) \cdot i_{\mathrm{DCT}} \cdot i_{\mathrm{a}} \cdot \eta_{\mathrm{t}} \\ \omega_{\mathrm{m}} = \omega_{\mathrm{e}} \\ T_{\mathrm{w}} - T_{\mathrm{L}} = I_{\mathrm{w}} \cdot \dot{\omega}_{\mathrm{w}} \end{cases} \tag{15}$$

The engine torque, ISG motor torque and clutch

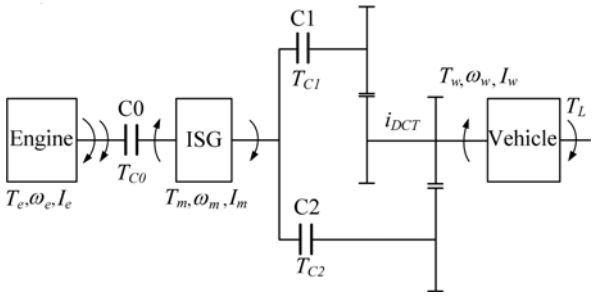

Figure 9. Dynamic model of engine starting.

transmitted torque in Equations (14) and (15) can be derived from the proposed dynamic models in Sections 2 ~ 4, respectively, which take the dynamic characteristics into consideration during the engine starting process.

5.2. Coordinated Control Strategy for Engine Starting Process

During the mode transition from electric driving mode to engine driving mode, the ISG motor will not only provide the driving torque for vehicle, but also an additional torque to overcome the engine drag torque. Therefore, the coordinated control strategy of the engine, the ISG motor and the main clutch is very important to ensure engine starting quickly and smoothly. The control flow chart of mode transition from electric driving mode to engine driving mode is shown in Figure 10. The coordinated control strategy has been divided into six phases and described in detail as follows.

1) The FHEV operates on electric driving mode and the motor target output torque T_{m_tar} in this phase is calculated by Equation (16).

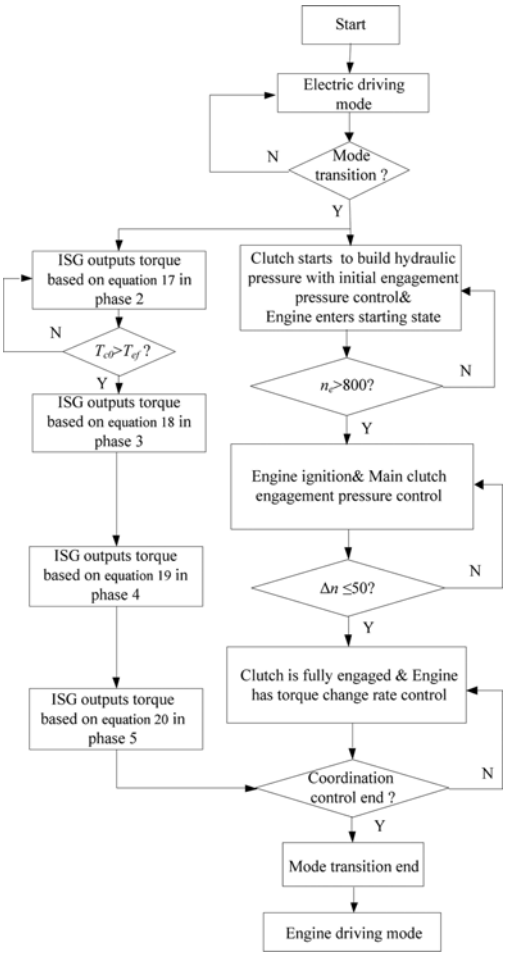

Figure 10. Control flow chart of the engine starting while driving.

$$T_{m\_tar} = T_{req} + J_{driven}\dot{\omega}_m \tag{16}$$

where, T_{m_tar} is the target output torque of ISG motor, T_{req} is the real-time required torque and J_{driven} is the equivalent moment of inertia of system converted to the main clutch driven plate.

2) After receiving the mode transition command from Vehicle Control Unit (VCU), the main clutch starts to engage so that the ISG motor can crank the engine. At the initial stage of engagement, the main clutch transmitted torque T_{c0} is less than engine drag torque T_{ef} and engine is stall. The output torque of ISG motor is needed to increase to overcome engine drag torque and the motor target output torque T_{m_tar} in this phase is calculated by Equation (17).

$$T_{m\_tar} = T_{req} + T_{c0} + J_{driven}\dot{\omega}_m \tag{17}$$

3) In this phase, the hydraulic cylinder pressure of main clutch increases gradually until the main clutch is slipping. The main clutch transmitted torque increases proportionally as the main clutch plate pressure increases. The coordinated ISG torque control has been introduced to compensate for the main clutch torque. Theoretically, if the ISG compensation torque is equal to the main clutch torque at any time, the engine starting process will achieve high performance in terms of smoothness. Therefore, the control strategy of ISG torque compensation for engine starting is mainly decided by the main clutch torque and its changing rate. After the main clutch transmitted torque is bigger than engine drag torque, the engine starts to rotate. The motor target output torque T_{m_tar} in this phase is calculated by Equation (18).

$$T_{m\_tar} = T_{req} + T_{ef} + J_{droven}\dot{\omega}_m + J_{driving}\dot{\omega}_e \tag{18}$$

4) When the engine speed reaches the ignition speed at 800 r/min, the engine ignites and the engine speed increases rapidly. After the engine ignition, it order to avoid the excessive driving torque, the ISG motor torque decreases rapidly as the engine torque increases. With the coordinated control of the main clutch and ISG motor, the engine speed will reach the target speed the same as the motor speed rapidly. Therefore, the output torque fluctuation of powertrain system will be reduced to a large extent. The motor target output torque T_{m_tar} in this phase is calculated by Equation (19).

$$T_{m\_tar} = T_{req} + T_e + J_{driven}\dot{\omega}_m + J_{driving}\dot{\omega}_e \tag{19}$$

5) When the difference speed between clutch driving and driven plates is less than a pre-set value, which can be calibrated in the actual control process (in this paper, this value is set as 50 r/min), the clutch engages as quickly as possible due to its limited influence to the fluctuation of output torque. After the main clutch engagement is finished, the motor torque continues to reduce as the engine torque increases. The ISG motor compensates the difference between the engine torque and the target torque until the driving torque is only provided by engine. The

motor target output torque T_{m_tar} in this phase is calculated by Equation (20).

$$T_{m\_tar} = T_{req} - T_e + (J_{driven} + J_{driving})\dot{\omega}_m \quad (20)$$

6) After accomplishment of the mode transition from driving mode electric to engine driving mode, the FHEV vehicle is driven by engine alone.

6. ANALYSIS OF SIMULATION AND BENCH TEST

According to the FHEV powertrain system dynamic models and the proposed coordinated control strategy, the simulation model of FHEV mode transition has been established based on the Matlab/Simulink platform, and then the mode transition from electric driving mode to engine driving mode and engine starting process simulation have been accomplished. At last, the bench test has been established to verify the simulation results.

6.1. Simulation Analysis

The simulation results of mode transition from electric driving mode to engine driving mode are shown in Figure 11. When the main clutch transmitted torque is smaller than engine drag torque T_{ef}, engine crankshaft will keep stationary state and engine transmitted torque is zero. At time of 6.15 s, engine starts to rotate with engine drag torque. At time of 6.41 s, the engine speed reaches 800 r/min. Then, engine ignites and starts to output driving torque. When engine speed reaches ISG motor speed roughly, the main clutch engages rapidly. After the clutch engagement is accomplished, ISG motor continues to compensate the difference between the engine torque and the target torque until engine output torque reaches the target torque. The duration of mode transition is 1.26 s and the maximum impact of vehicle is – 7.5 m/s^3. In Figure 11, the ISG motor torque decreases rapidly after the ignition with some fluctuation of torque due to the delay characteristics of PMSM with abrupt unloading. The hydraulic cylinder control pressure changes according to the designed principle, which can reduce the impact of

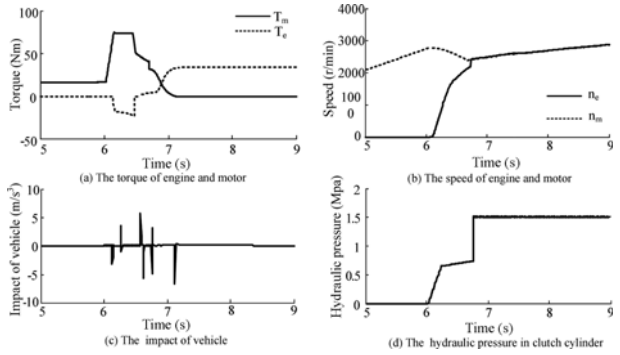

Figure 11. Simulation results of the engine starting based on dynamic modeling.

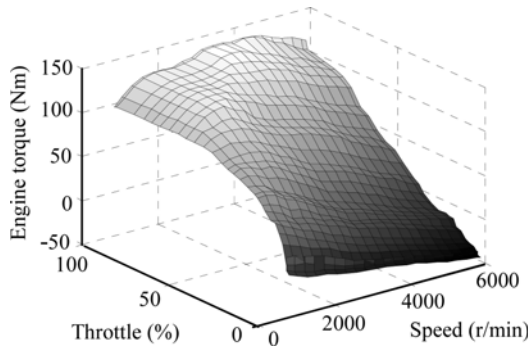

Figure 12. Engine output torque model.

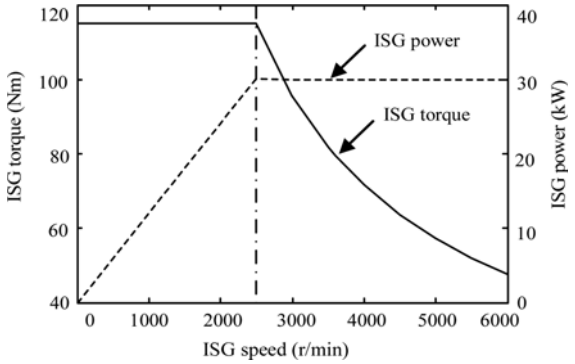

Figure 13. ISG motor characteristics.

vehicle powertrain system during the engagement. The effectiveness of coordinated control strategy based on dynamic characteristics of powertrain system is validated through the simulation results.

Moreover, the comparison for mode transition between traditional modeling and dynamic modeling has been carried out. In the traditional model, engine and ISG motor are both numerical model the main clutch model is built without considering the dynamic characteristics of actuator. The engine torque T_e is a function of engine speed n_e and throttle plate angle α as shown in the Figure 12 and the ISG motor characteristics in terms of torque and power are shown in the Figure 13. The simulation results of mode transition based on traditional modeling from electric driving mode to engine driving mode is described in Figure 14.

As shown in the Figure 14, the engine and ISG motor both can follow the target torque steadily during the whole mode transition. During the mode transition, the maximum impact of vehicle is 7.5 m/s^3. The duration of mode transition is 0.87 s, which is shorter than the mode transition based on dynamic modeling. The extra time approximately equals to the sum of dynamic response time of key components, which shows the dynamic characteristics of powertrain system can be accurately simulated through dynamic modeling. Meanwhile, it's apparent the simulation curves based on traditional modeling of powertrain system

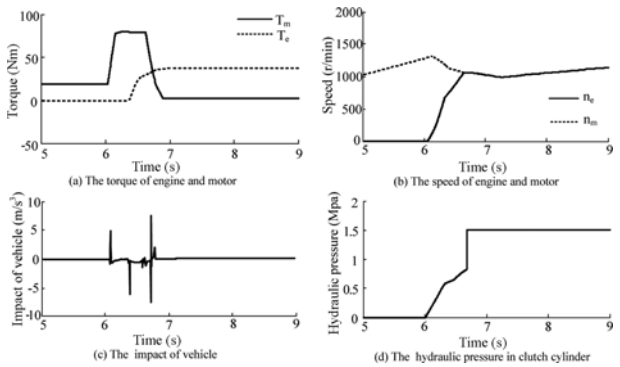

Figure 14. Simulation results of the engine starting while driving based on traditional modeling.

are smoother, which can't represent the actual situation of engine starting process. Therefore, the simulation results of dynamic modeling reflect the performance of mode transition more accurately in terms of the response and smoothness.

6.2. Bench Test Analysis

In order to further verify the accuracy of engine starting during mode transition based on dynamic modeling, the engine starting during mode transition bench test platform has been built using the rapid prototype developing system, which is developed by Matlab/Simulink platform and dSPACE software.

The bench test results of mode transition from electric driving mode to engine driving mode are described as Figure 15. The mode transition begins at time of 22 s. During the mode transition, the maximum impact of vehicle is 6.8 m/s^3 and the duration of mode transition is 2.1 s. Compared with the simulation results of mode transition based on dynamic modeling, the simulation curves is highly agreeable with that of test curves except that there is a little bit delay of test results. It is because that the signal processing time hasn't been take into consideration. The torque of engine and motor, the speed of engine and motor, hydraulic cylinder pressure have almost the same tendency with the bench test results during the mode transition,

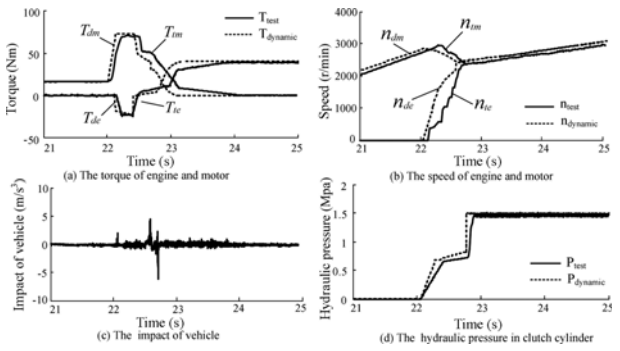

Figure 15. Bench test results of the engine starting.

which verifies the effectiveness of engine starting control for a FHEV based on system dynamic characteristics.

7. CONCLUSION

(1) This paper focuses on the modeling and control of engine starting for a full hybrid electric vehicle based on system dynamic characteristics. The dynamic models of key components of powertrain system of FHEV have been proposed, including the engine, the motor and the main clutch, which provide a foundation for the research of coordinated control strategy of engine starting.

(2) The dynamic model of powertrain system for engine starting process during electric driving mode has been established and the coordinated control strategy of engine starting during electric driving mode has been proposed. The motor target output torque has been derived at each phase according to the dynamic model of powertrain system of the FHEV, which is crucial to realize the successful mode transition.

(3) The simulation models of FHEV during mode transition have been established based on the Matlab/Simulink platform. The bench test platform has also been built up. The effectiveness of the coordinated control strategies based on system dynamic characteristics have been validated by the comparison between simulation results and the bench test data, which provide a theoretical basis for developing the mode transition strategy and improving the mode transition performance.

ACKNOWLEDGEMENT–The work presented in this paper is funded by the China Postdoctoral Science Foundation (No. 2016M602925XB), the Fundamental Research Funds for the Central Universities (No. CDJZR14110005), the Key Laboratory of Advanced Manufacture Technology for Automobile Parts, Ministry of Education (No. 2016KLMT06) and the Chongqing Research Program of Basic Research and Frontier Technology (No. cstc2013jcyjA60004).

REFERENCES

Ahn, K. and Cha, S. W. (2008). Developing mode shift strategies for a two-mode hybrid powertrain with fixed gears. *SAE Int. J. Passenger Cars Mechanical Systems* **1**, **1**, 285–292.

Asl, H. A., Saeedi, M., Fraser, R., Goossens, P. and Mcphee, J. (2013). Mean value engine model including spark timing for powertrain control application. *SAE Paper No*. 2013-01-0247.

Broomhead, T., Manzie, C., Brear, M. and Hield, P. (2015). Model reduction of diesel mean value engine models. *SAE Paper No*. 2015-01-1248.

Cho, B. H., Oh, J. S. and Lee, W. H. (2002). Modeling of pulse width modulation pressure control system for automatic transmission. *SAE Paper No*. 2002-01-1257.

He, Y. and Lin, C. C. (2007). Development and validation of a mean value engine model for integrated engine and control system simulation. *SAE Paper No*. 2007-01-1304.

Hendricks, E. and Sorenson, S. C. (1990). Mean value modelling of spark ignition engines. *SAE Paper No*. 900616.

Hendricks, E. and Vesterholm, T. (1992). The analysis of mean value SI engine models. *SAE Paper No*. 920682.

Hendricks, E., Chevalier, A., Jensen, M., Sorenson, S. C., Trumpy, D. and Asik, J. (1996). Modelling of the intake manifold filling dynamics. *SAE Paper No*. 960037.

Hendricks, E., Vesterholm, T. and Sorenson, S. C. (1992). Nonlinear, closed loop, SI engine control observers. *SAE Paper No*. 920237.

Ke, L., Zhang, C., Cui, N. and Ma, M. (2008). High dynamic response control of induction motor in high-speed region for electric vehicle drive system. *IEEE Power Electronics Specialists Conf*., 3093–3097.

Kim, H., Kim, J., Lee, H., Kim, H., Kim, J. and Lee, H. (2011). Mode transition control using disturbance compensation for a parallel hybrid electric vehicle. *Proc. Institution of Mechanical Engineers, Part D: J. Automobile Engineering* **225**, **2**, 150–166.

Kim, T. and Vodyakho, O. (2009). Brushless PM machine drive in electric and hybrid electric vehicles based on the space vector current control. *Int. J. Automotive Technology* **10**, **6**, 711–717.

Lee, J. H., Lee, H. J. and Sunwoo, M. (2014). Nonlinear sliding mode observer for exhaust manifold pressure estimation in a light-duty diesel engine. *Int. J. Automotive Technology* **15**, **3**, 377–386.

Liu, J. R., Jin, B., Xie, Y. J., Chen, Y. and Weng, Z. T. (2009). Research on the electro-hydraulic variable valve actuation system based on a three-way proportional reducing valve. *Int. J. Automotive Technology* **10**, **1**, 27–36.

Ma, Y., Huang, K., Xiang, C. and Wang, W. (2015). A control strategy to reduce torque variation for dual-mode power-split hybrid electric vechile during mode shift. *IEEE Int. Conf., Modelling, Identification and Control (ICMIC)*.

Manyala, J. and Atashbar, M. (2013). Electromagnetic actuator dynamic response prediction for an automated mechanical transmission. *SAE Int. J. Commercial Vehicles* **6**, **1**, 1–9.

Meng, F., Zhang, H., Cao, D. and Chen, H. (2015). System modeling and pressure control of a clutch actuator for heavy-duty automatic transmission systems. *IEEE Trans. Vehicular Technology* **65**, **7**, 4865–4874.

Meng, Z., Chen, R. and An, Y. (2013). Direct torque control of interior permanent magnet synchronous motors based on sensorless control and fuzzy controller. *Int. Conf. Intelligent Human-Machine Systems & Cybernetics, IEEE Computer Society* **756**, **759**, 556–559.

Oh, S. C. (2005). Evaluation of motor characteristics for hybrid electric vehicles using the hardware-in-the-loop concept. *IEEE Trans. Vehicular Technology* **54**, **3**, 817–824.

Smith, A., Bucknor, N., Yang, H. and He, Y. (2011). Controls development for clutch-assisted engine starts in a parallel hybrid electric vehicle. *SAE Paper No*. 2011-01-0870.

Somayajula, D., Meintz, A. and Ferdowsi, M. (2009). Designing efficient hybrid electric vehicles. *IEEE Vehicular Technology Magazine* **4**, **2**, 65–72.

Song, M., Oh, J. and Kim, H. (2012). Engine clutch control algorithm during mode change for parallel hybrid electric vehicle. *IEEE Vehicle Power and Propulsion Conf*., 1118–1121.

Wu, H., Wang, X., Winsor, R. and Baumgard, K. (2011). Mean value engine modeling for a diesel engine with gt-power 1d detail model. *SAE Paper No*. 2011-01-1294.